Electronic Supplementary Material

CD137 agonist potentiates the abscopal efficacy of nanoparticle-based photothermal therapy for melanoma

Preethi Bala Balakrishnan[1], Debbie K. Ledezma[2], Juliana Cano-Mejia[1], Jaclyn Andricovich[2], Erica Palmer[3], Vishal A. Patel[4], Patricia S. Latham[5], Eric S. Yvon[1], Alejandro Villagra[3], Rohan Fernandes[1,2,6] (✉), and Elizabeth E. Sweeney[3,6] (✉)

[1] *GW Cancer Center, Department of Medicine, School of Medicine and Health Sciences, George Washington University, Washington, DC 20052, USA*
[2] *The Institute for Biomedical Sciences, School of Medicine and Health Sciences, George Washington University, Washington, DC 20052, USA*
[3] *GW Cancer Center, Department of Biochemistry and Molecular Medicine, School of Medicine and Health Sciences, George Washington University, Washington, DC 20052, USA*
[4] *Department of Dermatology & Oncology, School of Medicine and Health Sciences, George Washington University, Washington, DC 20037, USA*
[5] *Department of Pathology, School of Medicine and Health Sciences, George Washington University, Washington, DC 20037, USA*
[6] *ImmunoBlue, Bethesda, MD 20817, USA*

Supporting information to https://doi.org/10.1007/s12274-021-3813-1

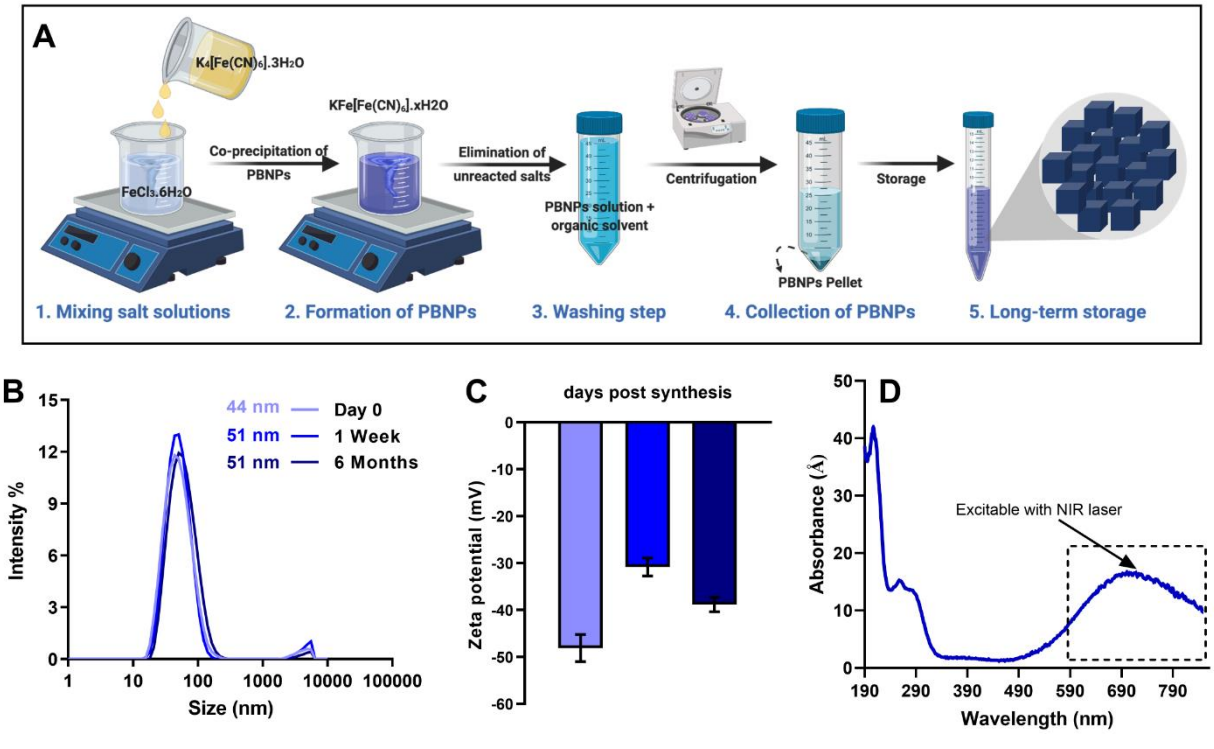

Address correspondence to Rohan Fernandes, rfernandes@gwu.edu; Elizabeth E. Sweeney, lizie@gwu.edu

TSINGHUA UNIVERSITY PRESS Springer

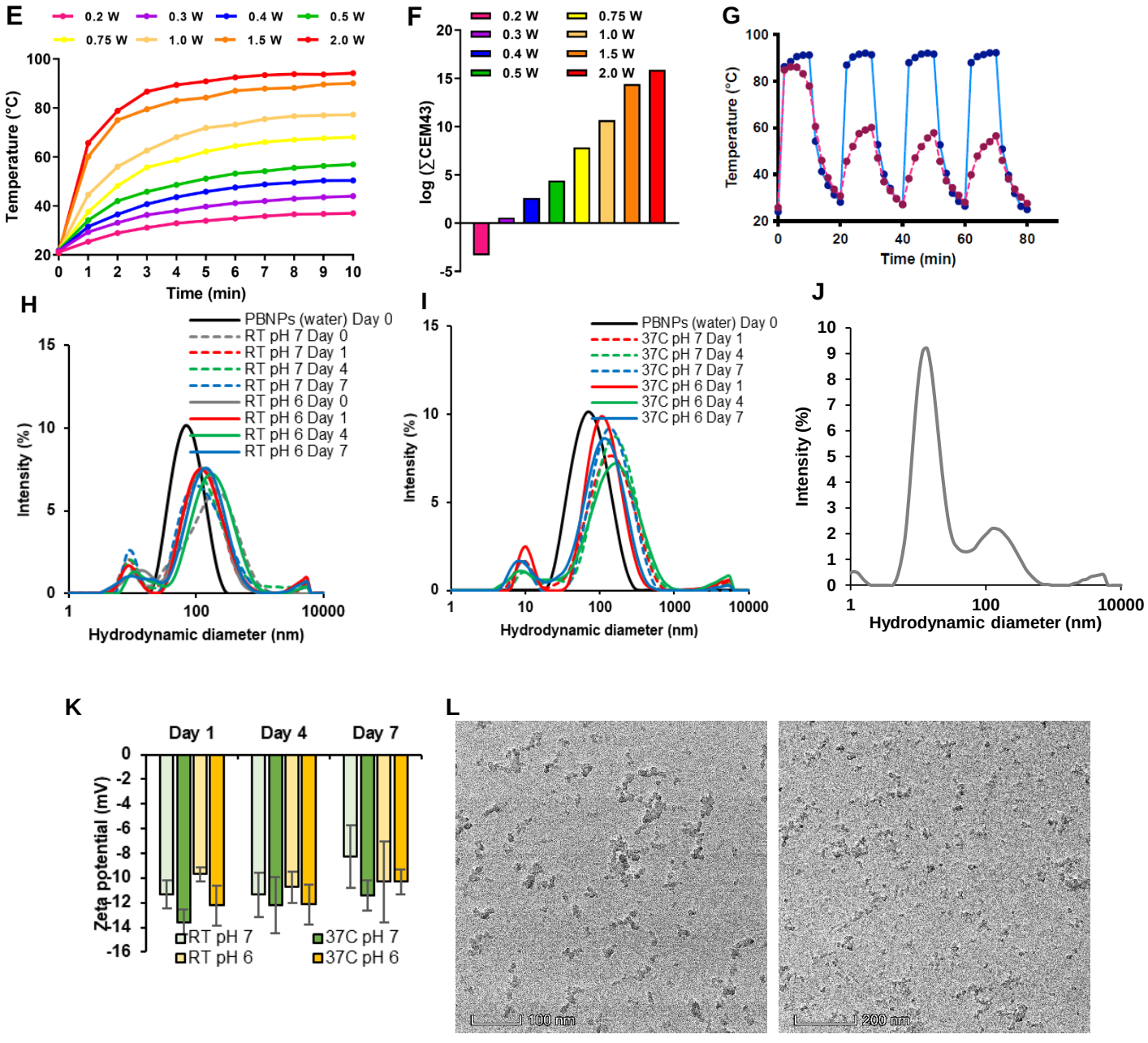

Figure S1 Synthesis and characterization of Prussian blue nanoparticles (PBNPs). A) PBNPs were prepared by a co-precipitation method using $FeCl_3.6H_20$ and $K_4[Fe(CN)_6].3H_2O$. The co-precipitated nanoparticles were washed to eliminate excess unreacted salts. B-C) Dynamic light scattering and zeta potential graphs show monodispersed PBNPs of size 50 nm that were negatively charged (< -30 mV) and stable over a time period of 6 months. D) UV-Vis-NIR spectrum of PBNPs shows a wide absorption peak ranging from 600 to > 800 nm, making them suitable for excitation using an 808 NIR laser for photothermal therapy. E-F) The heating of PBNPs by laser illumination is laser power dependent, as shown by (E) increasing temperature and (F) thermal dose (ΣCEM43) with laser powers ranging from 0.2 W to 2 W. G) 2 W PBNP-PTT identically heats PBNPs over four cycles of heating in water (blue), but cyclic heating in complete cell culture media with 10% FBS (purple) is less effective after the first cycle of PBNP-PTT. H) Hydrodynamic diameter distribution of PBNPs at pH 7 or pH 6 in complete cell culture media with 10% FBS at room temperature (RT) over seven days, as compared to PBNPs in water (black). I) Hydrodynamic diameter distribution of PBNPs at pH 7 or pH 6 in complete cell culture media with 10% FBS at 37˚ C (37C) over seven days, as compared to PBNPs in water (black). The peak representing smaller sizes (~10 nm) likely reflects media components (e.g. proteins in serum), and the increase in hydrodynamic diameter may be caused by a protein corona formed on the surface of PBNPs upon dispersion in serum-containing media. J) Representative hydrodynamic diameter distribution of PBNP-free complete cell culture media with 10% FBS (pH 6 at RT on Day 1), illustrating a peak ~10 nm as predicted. K) Zeta potential of PBNPs was measured in complete cell culture media with 10% FBS at room temperature (RT) or 37˚ C (37C) at pH 7 or 6 over seven days. L) Transmission electron microscopy (TEM) images illustrating the morphology of PBNPs. Scale bar = 100 nm (left) and 200 nm (right).

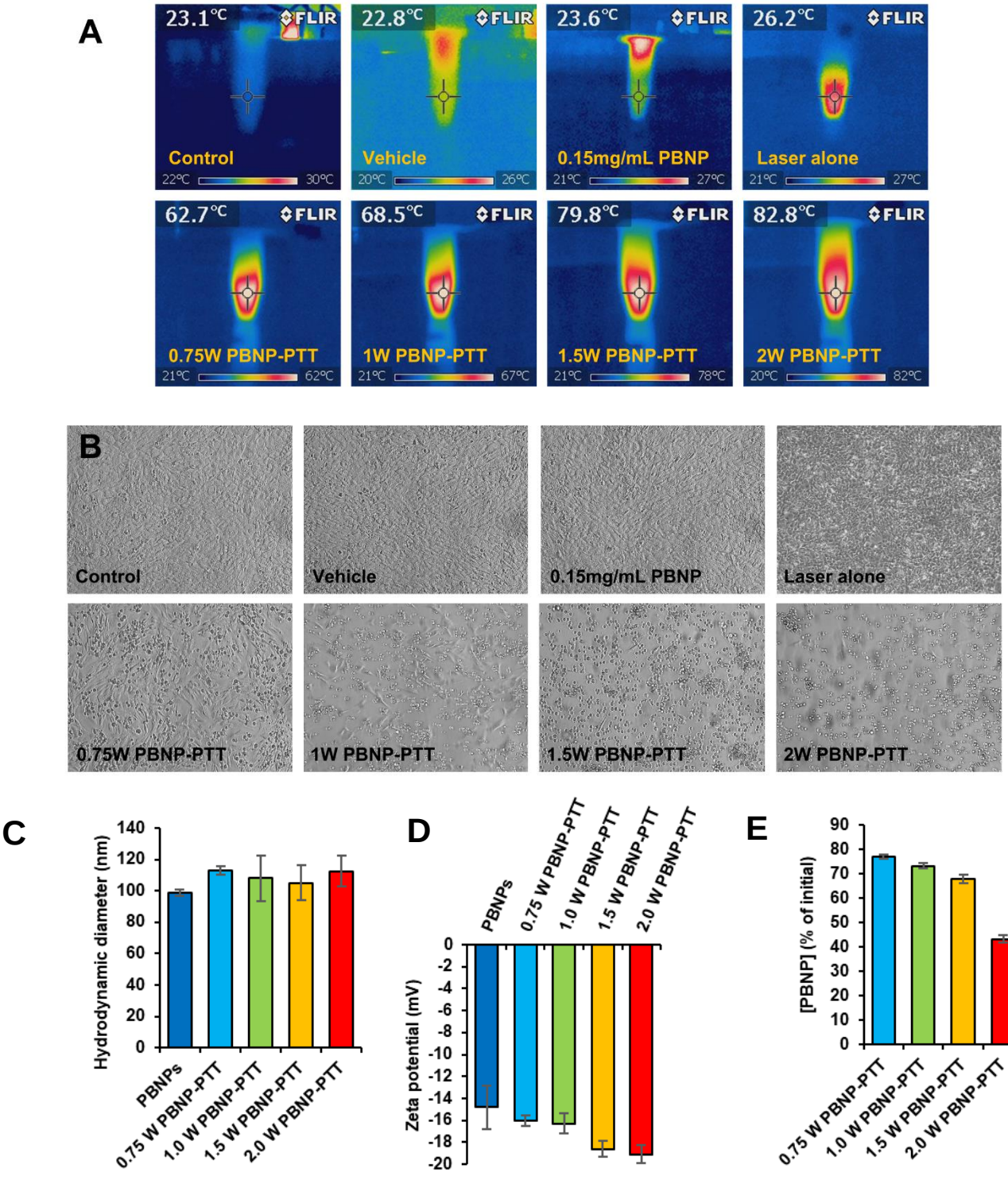

Figure S2. Physical characteristics of PBNP-PTT *in vitro*. A) Thermal images of SM1 murine melanoma cells treated with 0.15 mg mL^{-1} PBNPs and exposed to 10 min laser illumination. Each panel displays the thermal distribution (heat map) that indicates the maximum temperature reached while performing *in vitro* PBNP-PTT using different laser powers (0.75 W - 2 W). B) Bright-field images of SM1 cells 24 h post-PBNP-PTT shows increased dead and floating cells (loss of confluence) with increased temperature/laser power. Bright-field images were taken at 20X magnification using Leica DMi1 inverted light microscope. C) PBNP size distribution (hydrodynamic diameter) was measured after 10 min PBNP-PTT in media at varied thermal doses. D) PBNP surface charge (zeta potential) was measured after 10 min PBNP-PTT in media at varied thermal doses. E) As a measure of degradation, PBNP concentration was measured after 10 min PBNP-PTT at varied thermal doses. A thermal dose-dependent degradation of PBNPs was observed.

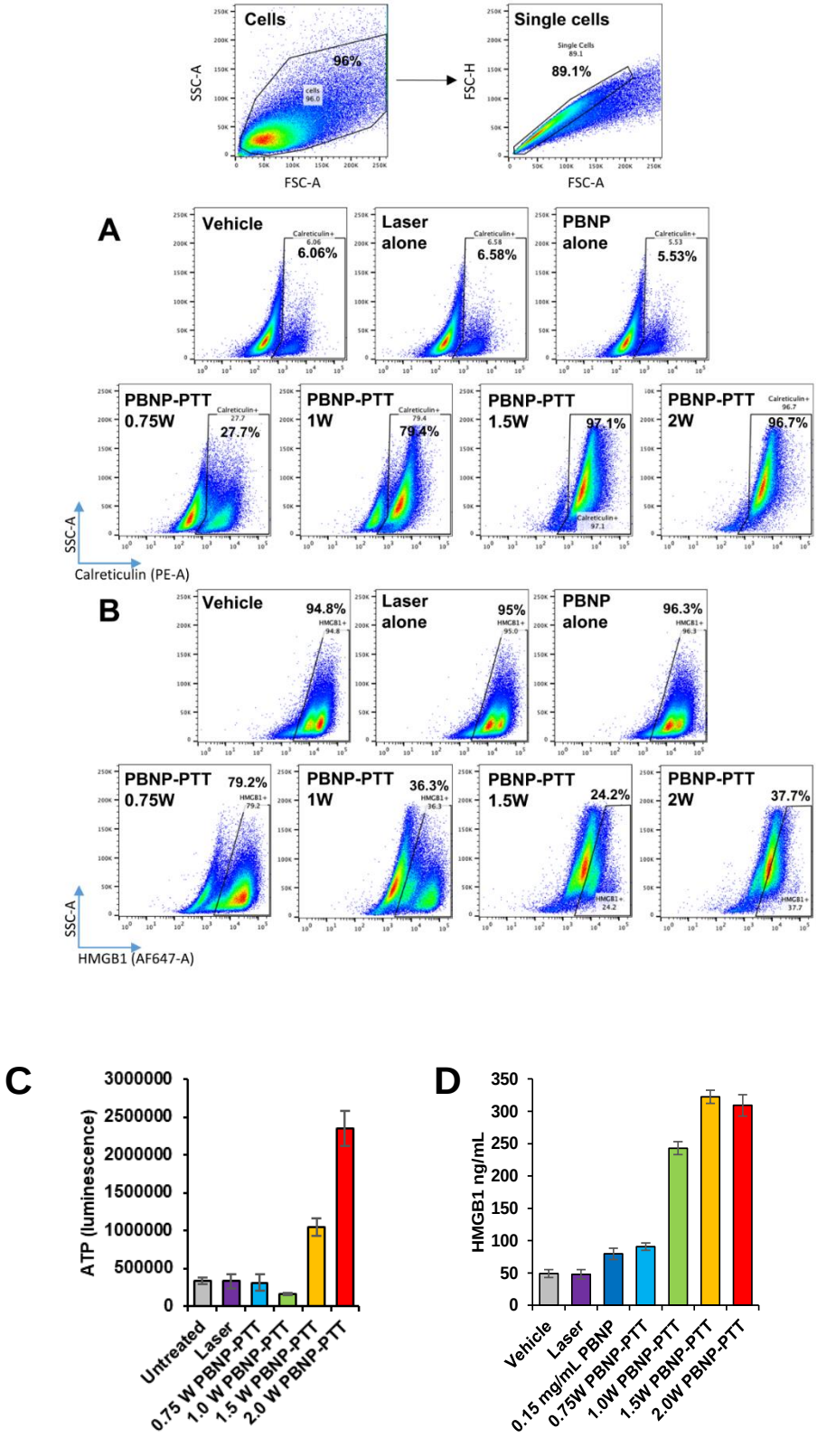

Figure S3 Analysis of SM1 cells for immunogenic cell death (ICD) markers. A-B) Scatter plots showing (A) an increase in surface calreticulin and (B) a decrease in intracellular levels of HMGB1 for SM1 cells treated with higher laser power, indicating the generation of ICD with increased laser power and thermal dose. C) Analysis of extracellular ATP in the supernatant of cell culture media after 10 min PBNP-PTT at varied thermal doses. Extracellular ATP was measured by the RealTime-Glo Extracellular ATP Assay (Promega) following the manufacturer's protocol. D) Analysis of extracellular HMGB1 in the supernatant of cell culture media after 10 min PBNP-PTT at varied thermal doses. Extracellular HMGB1 was measured by the HMGB1 Detection ELISA Kit (Chondrex) following the manufacturer's protocol.

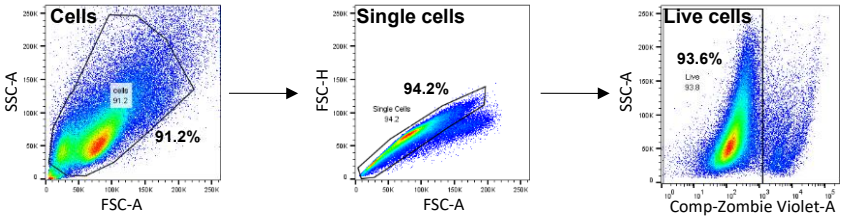
Cells
91.2%
SSC-A
FSC-A
Single cells
94.2%
FSC-H
FSC-A
Live cells
93.6%
SSC-A
Comp-Zombie Violet-A

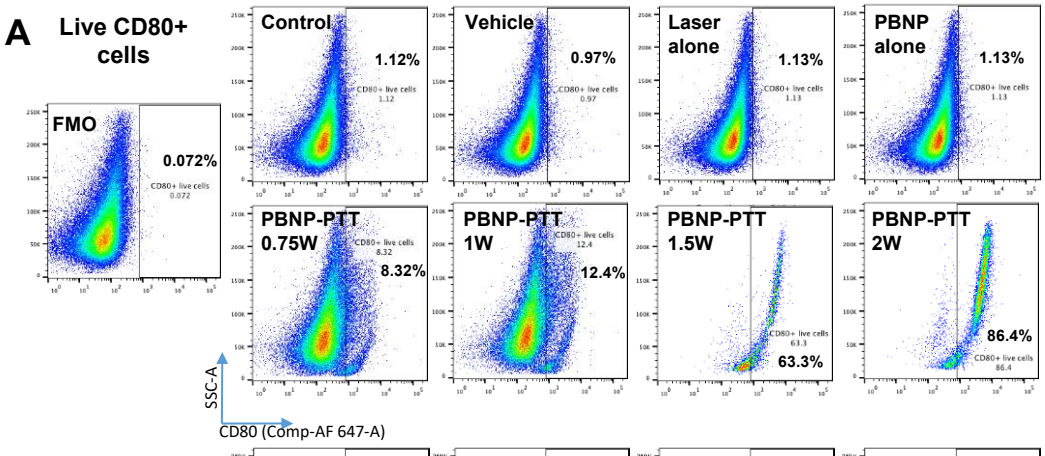
A
Live CD80+ cells
FMO
0.072%
Control
1.12%
Vehicle
0.97%
Laser alone
1.13%
PBNP alone
1.13%
PBNP-PTT 0.75W
8.32%
PBNP-PTT 1W
12.4%
PBNP-PTT 1.5W
63.3%
PBNP-PTT 2W
86.4%
SSC-A
CD80 (Comp-AF 647-A)

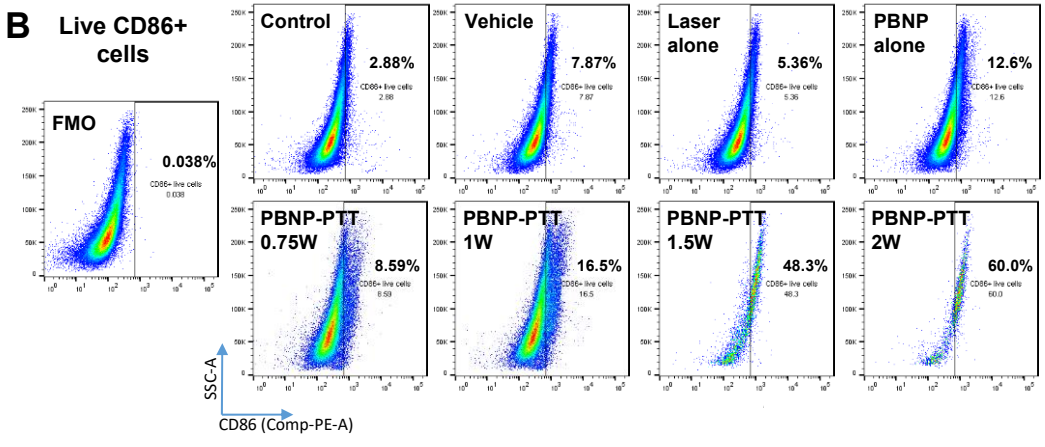
B
Live CD86+ cells
FMO
0.038%
Control
2.88%
Vehicle
7.87%
Laser alone
5.36%
PBNP alone
12.6%
PBNP-PTT 0.75W
8.59%
PBNP-PTT 1W
16.5%
PBNP-PTT 1.5W
48.3%
PBNP-PTT 2W
60.0%
SSC-A
CD86 (Comp-PE-A)

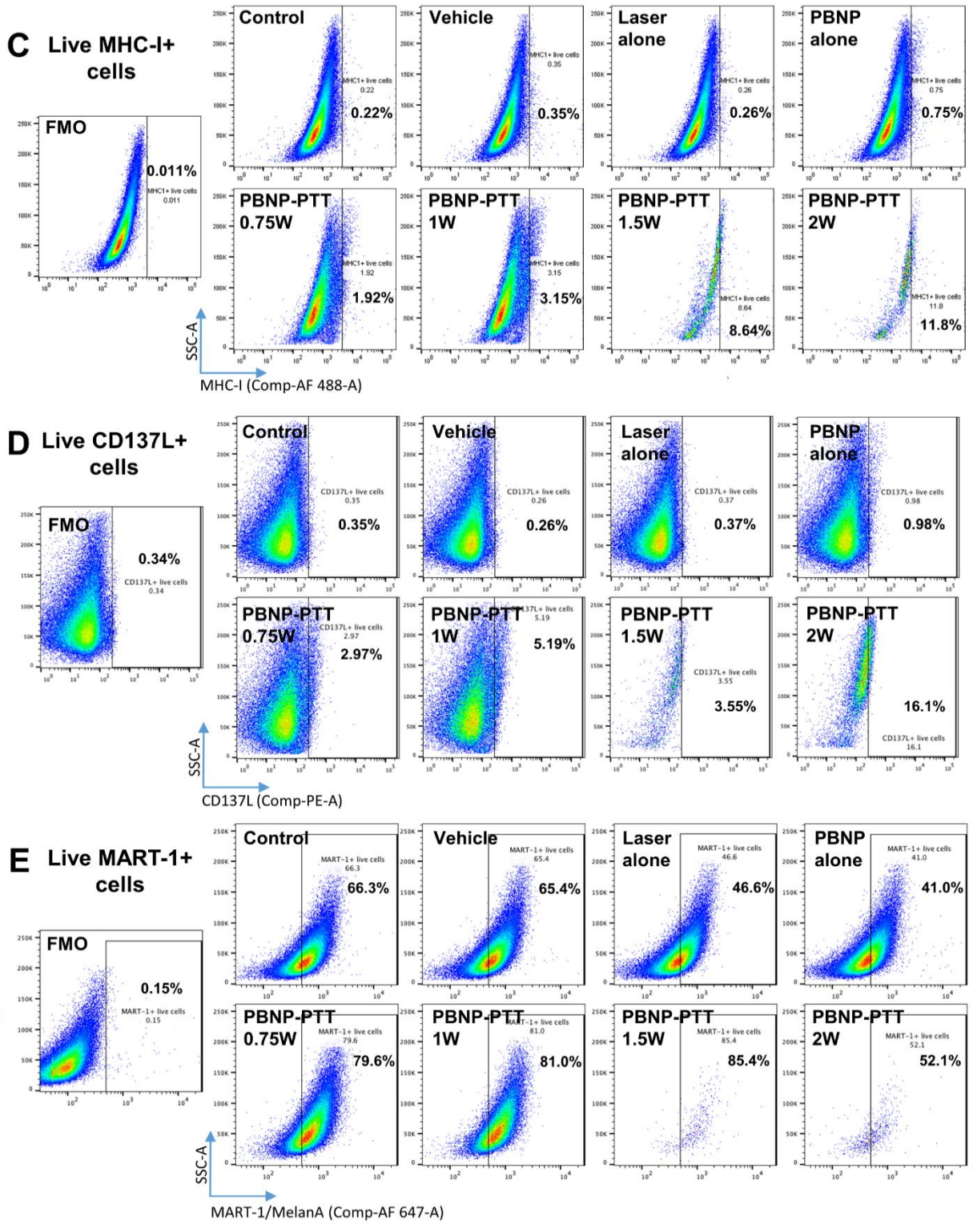

Figure S4 Flow cytometry analysis of SM1 cells for expression of immunostimulatory molecules after PBNP-PTT. A-E) Scatter plots showing increases in molecules associated with T cell stimulation, (A) CD80, (B) CD86, (C) MHC-I, (D) CD137L, and (E) Melanoma Antigen Recognized by T cells (MART-1) expressed on the surface of surviving SM1 cells treated with PBNP-PTT at varying laser powers, suggesting increased immunogenicity with increased laser power and thermal dose.

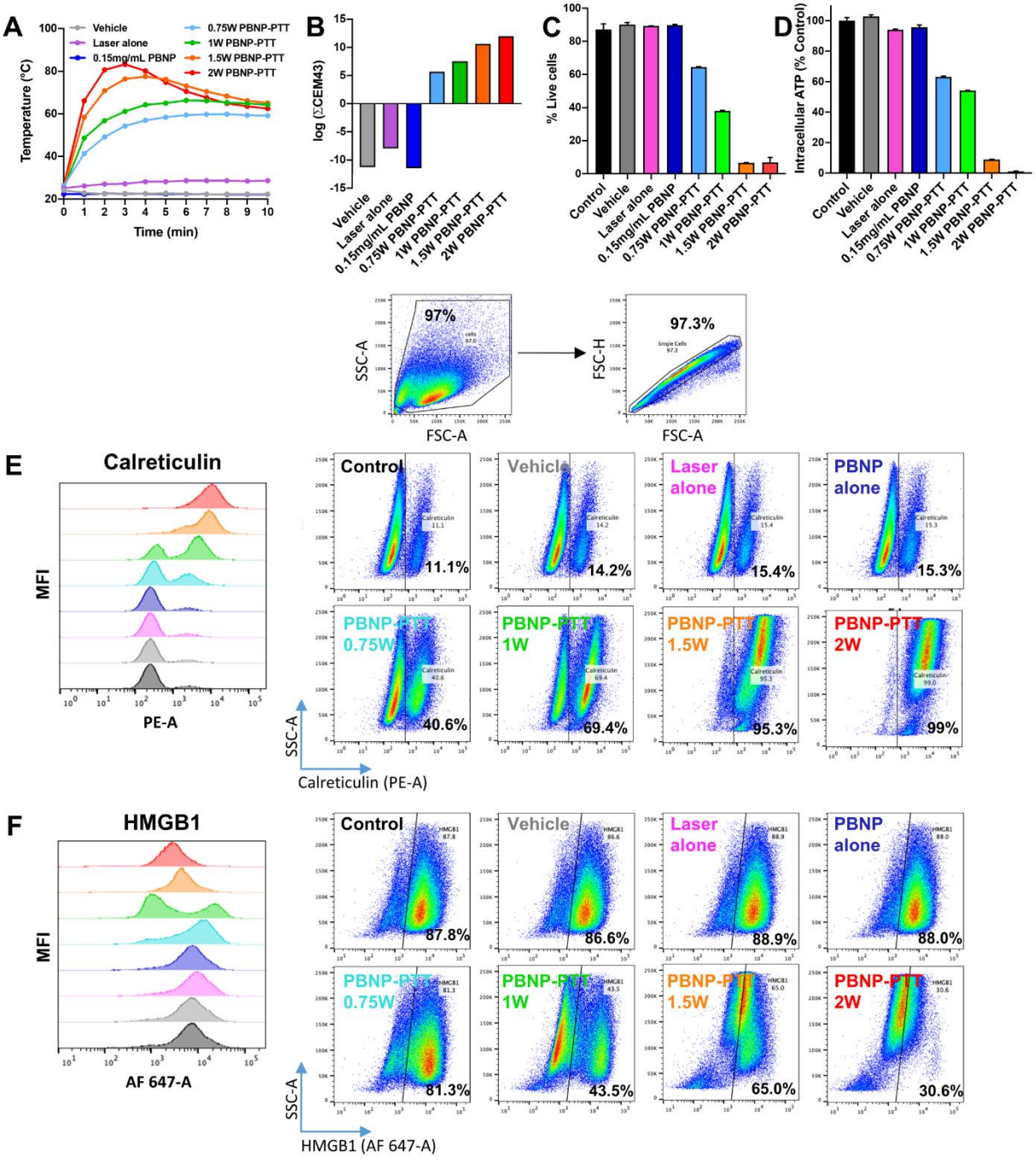
A
Vehicle
Laser alone
0.15mg/mL PBNP
0.75W PBNP-PTT
1W PBNP-PTT
1.5W PBNP-PTT
2W PBNP-PTT
Temperature (°C)
Time (min)
B
log (ΣCEM43)
Vehicle
Laser alone
0.15mg/mL PBNP
0.75W PBNP-PTT
1W PBNP-PTT
1.5W PBNP-PTT
2W PBNP-PTT
C
% Live cells
Control
Vehicle
Laser alone
0.15mg/mL PBNP
0.75W PBNP-PTT
1W PBNP-PTT
1.5W PBNP-PTT
2W PBNP-PTT
D
Intracellular ATP (% Control)
Control
Vehicle
Laser alone
0.15mg/mL PBNP
0.75W PBNP-PTT
1W PBNP-PTT
1.5W PBNP-PTT
2W PBNP-PTT
97%
SSC-A
FSC-A
97.3%
FSC-H
FSC-A
E
Calreticulin
MFI
PE-A
Control
11.1%
Vehicle
14.2%
Laser alone
15.4%
PBNP alone
15.3%
PBNP-PTT 0.75W
40.6%
PBNP-PTT 1W
69.4%
PBNP-PTT 1.5W
95.3%
PBNP-PTT 2W
99%
SSC-A
Calreticulin (PE-A)
F
HMGB1
MFI
AF 647-A
Control
87.8%
Vehicle
86.6%
Laser alone
88.9%
PBNP alone
88.0%
PBNP-PTT 0.75W
81.3%
PBNP-PTT 1W
43.5%
PBNP-PTT 1.5W
65.0%
PBNP-PTT 2W
30.6%
SSC-A
HMGB1 (AF 647-A)

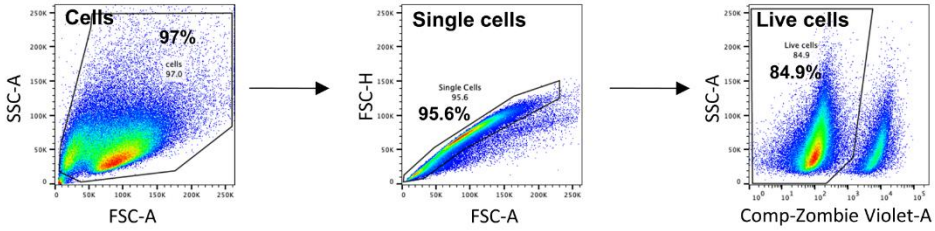
Cells
97%
SSC-A
FSC-A
Single cells
95.6%
FSC-H
FSC-A
Live cells
84.9%
SSC-A
Comp-Zombie Violet-A

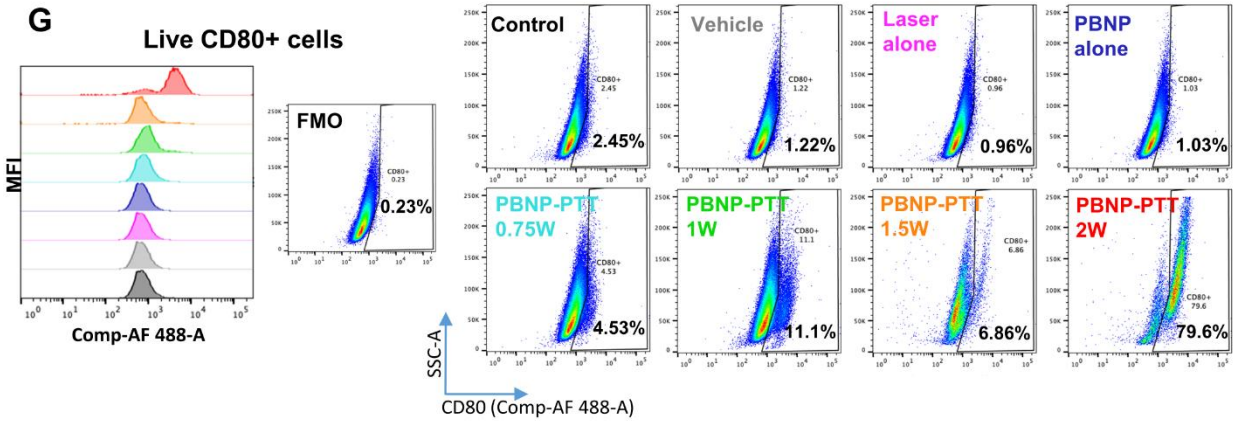
G
Live CD80+ cells
MFI
Comp-AF 488-A
FMO
0.23%
Control
2.45%
Vehicle
1.22%
Laser alone
0.96%
PBNP alone
1.03%
PBNP-PTT 0.75W
4.53%
PBNP-PTT 1W
11.1%
PBNP-PTT 1.5W
6.86%
PBNP-PTT 2W
79.6%
SSC-A
CD80 (Comp-AF 488-A)

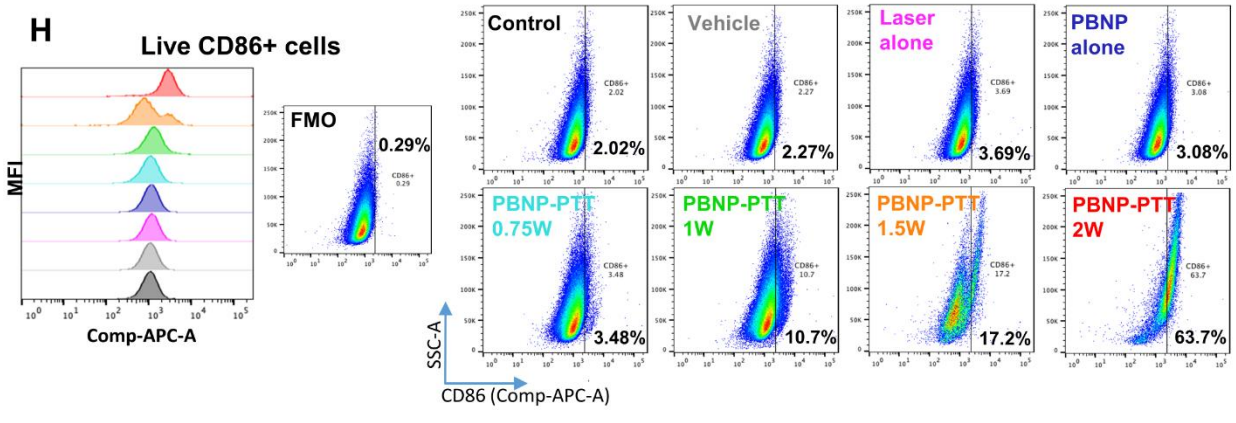
H
Live CD86+ cells
MFI
Comp-APC-A
FMO
0.29%
Control
2.02%
Vehicle
2.27%
Laser alone
3.69%
PBNP alone
3.08%
PBNP-PTT 0.75W
3.48%
PBNP-PTT 1W
10.7%
PBNP-PTT 1.5W
17.2%
PBNP-PTT 2W
63.7%
SSC-A
CD86 (Comp-APC-A)

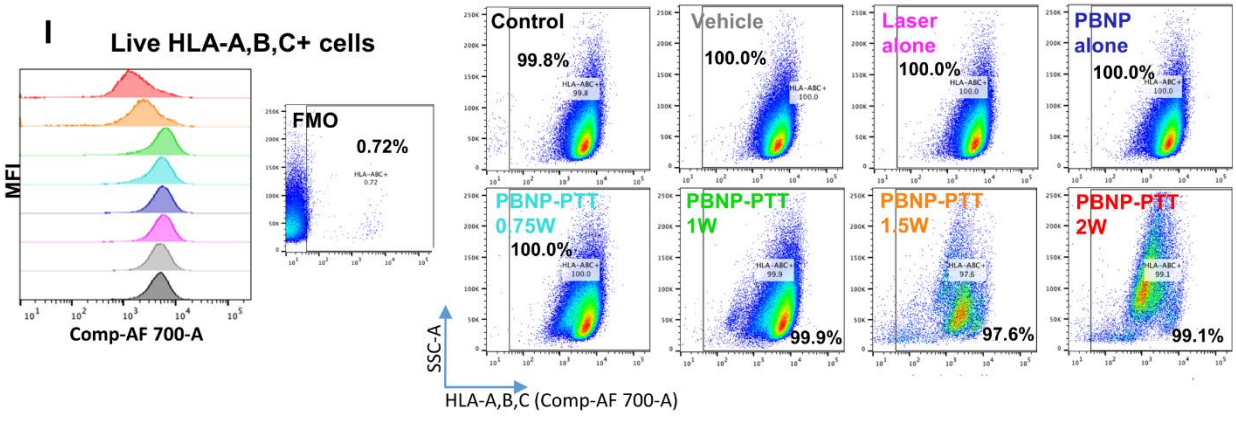
I
Live HLA-A,B,C+ cells
MFI
Comp-AF 700-A
FMO
0.72%
Control
99.8%
Vehicle
100.0%
Laser alone
100.0%
PBNP alone
100.0%
PBNP-PTT 0.75W
100.0%
PBNP-PTT 1W
99.9%
PBNP-PTT 1.5W
97.6%
PBNP-PTT 2W
99.1%
SSC-A
HLA-A,B,C (Comp-AF 700-A)

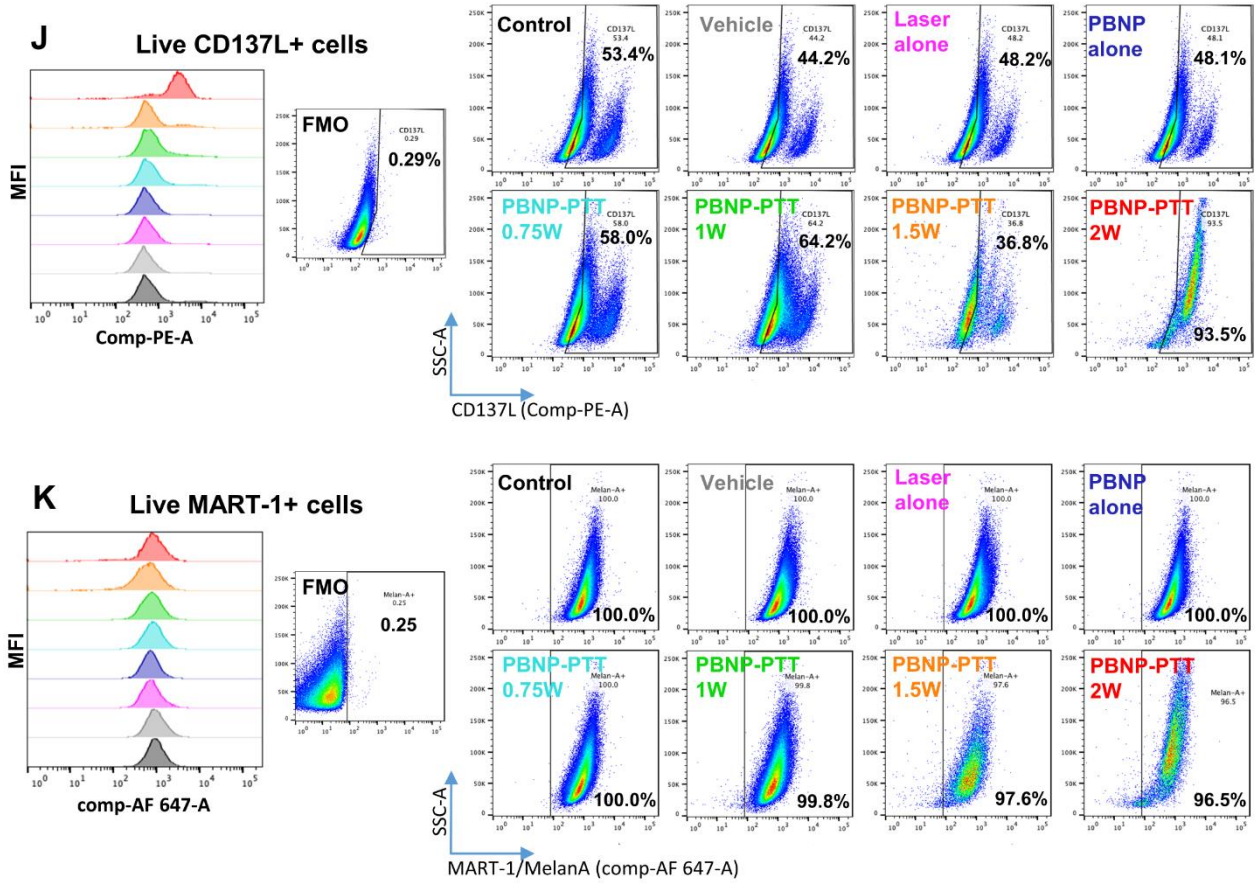

Figure S5 Analysis of WM9 human melanoma cells for expression of ICD markers and immunostimulatory molecules after PBNP-PTT. A) Temperature curve showing consistent increase in temperature in a laser-power dependent manner, with the highest temperature of 85.5 °C reached with 2 W PBNP-PTT. B) CEM43 graph indicating an increase in thermal dose in a laser-power dependent manner. C) Viability assay by flow cytometry shows WM9 cell death in a thermal-dose dependent manner. D-F) Analysis of molecules associated with ICD (ATP, calreticulin, and HMGB1) showed (D) increased ATP release (indicated by lower intracellular ATP), (E) increased surface calreticulin, and (F) decreased intracellular HMGB1 in a thermal dose-dependent manner. G-K) Flow cytometry analysis showing an increase in molecules associated with T cell stimulation, (G) CD80, (H) CD86, (I) HLA-class I (HLA-A,B,C), (J) CD137L, and (K) MART-1 expressed on surface of surviving WM9 human melanoma cells treated with PBNP-PTT at varying laser powers, suggesting increased immunogenicity with increased laser power and thermal dose, consistent with the SM1 murine melanoma model.

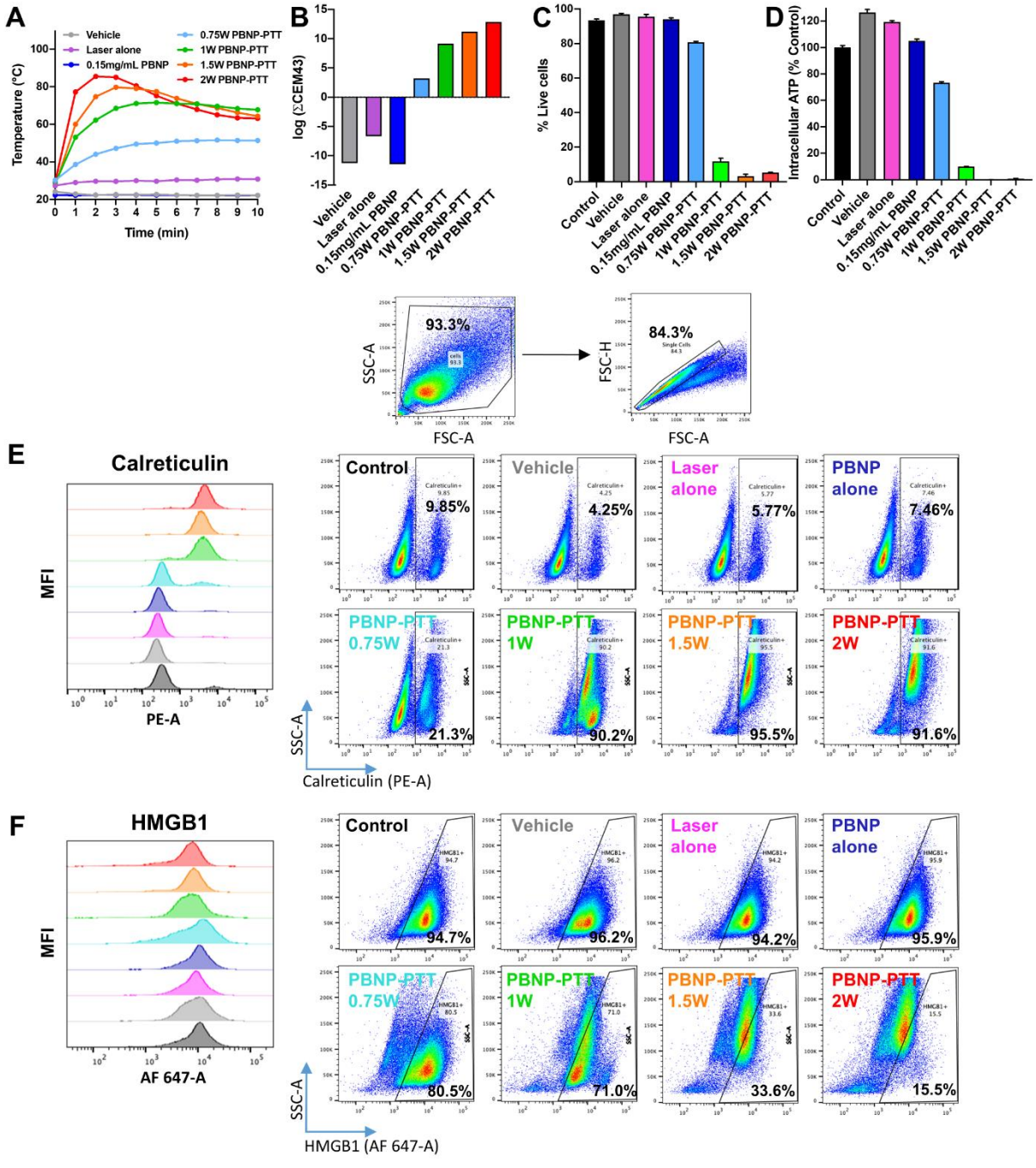
A
Vehicle
Laser alone
0.15mg/mL PBNP
0.75W PBNP-PTT
1W PBNP-PTT
1.5W PBNP-PTT
2W PBNP-PTT
Temperature (°C)
Time (min)
B
log (ΣCEM43)
Vehicle
Laser alone
0.15mg/mL PBNP
0.75W PBNP-PTT
1W PBNP-PTT
1.5W PBNP-PTT
2W PBNP-PTT
C
% Live cells
Control
Vehicle
Laser alone
0.15mg/mL PBNP
0.75W PBNP-PTT
1W PBNP-PTT
1.5W PBNP-PTT
2W PBNP-PTT
D
Intracellular ATP (% Control)
Control
Vehicle
Laser alone
0.15mg/mL PBNP
0.75W PBNP-PTT
1W PBNP-PTT
1.5W PBNP-PTT
2W PBNP-PTT
93.3%
SSC-A
FSC-A
84.3%
FSC-H
FSC-A
E
Calreticulin
MFI
PE-A
Control
9.85%
Vehicle
4.25%
Laser alone
5.77%
PBNP alone
7.46%
PBNP-PTT 0.75W
21.3%
PBNP-PTT 1W
90.2%
PBNP-PTT 1.5W
95.5%
PBNP-PTT 2W
91.6%
SSC-A
Calreticulin (PE-A)
F
HMGB1
MFI
AF 647-A
Control
94.7%
Vehicle
96.2%
Laser alone
94.2%
PBNP alone
95.9%
PBNP-PTT 0.75W
80.5%
PBNP-PTT 1W
71.0%
PBNP-PTT 1.5W
33.6%
PBNP-PTT 2W
15.5%
SSC-A
HMGB1 (AF 647-A)

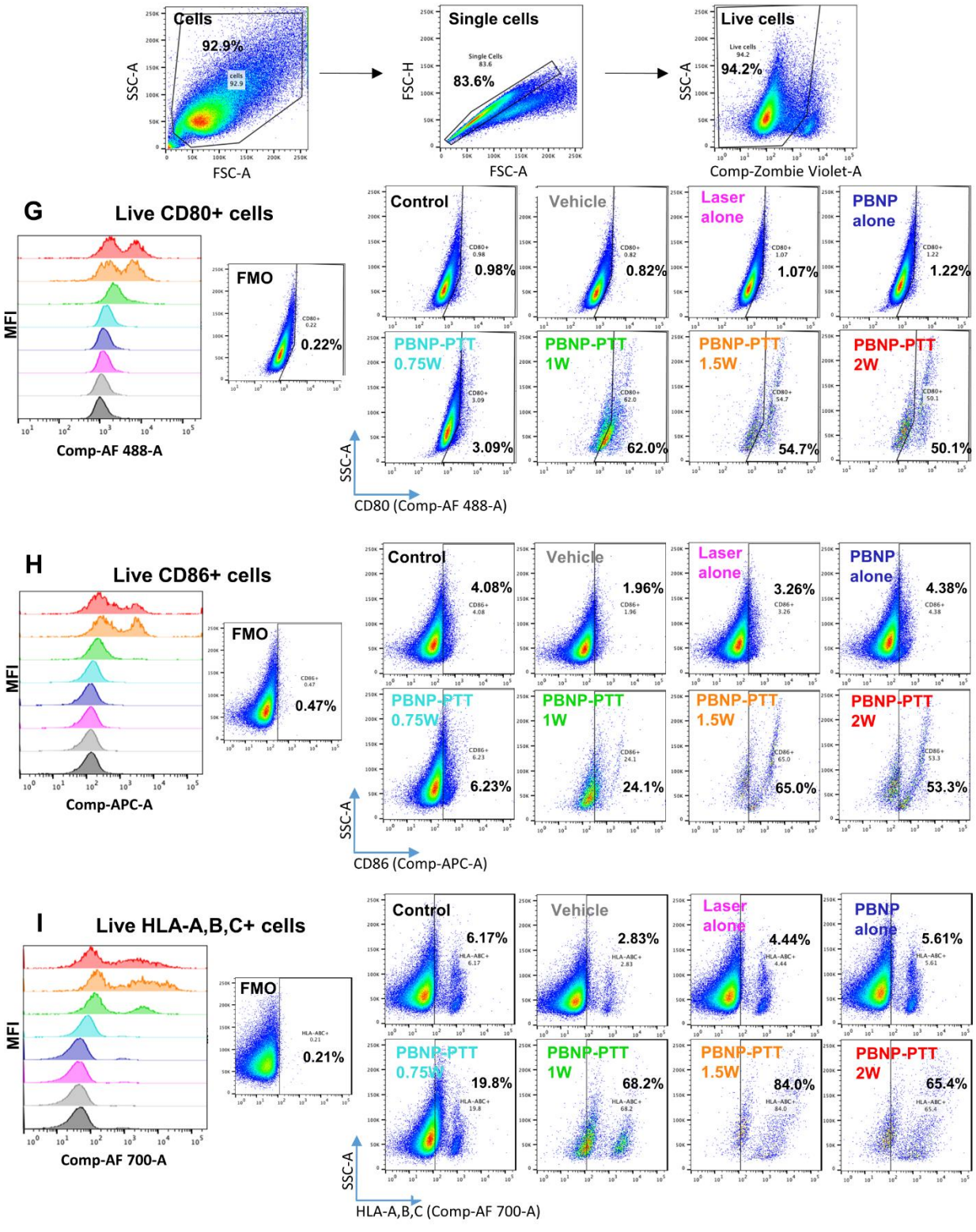
Cells
92.9%
SSC-A
FSC-A
Single cells
83.6%
FSC-H
FSC-A
Live cells
94.2%
SSC-A
Comp-Zombie Violet-A
G
Live CD80+ cells
MFI
Comp-AF 488-A
FMO
0.22%
Control
0.98%
Vehicle
0.82%
Laser alone
1.07%
PBNP alone
1.22%
PBNP-PTT 0.75W
3.09%
PBNP-PTT 1W
62.0%
PBNP-PTT 1.5W
54.7%
PBNP-PTT 2W
50.1%
SSC-A
CD80 (Comp-AF 488-A)
H
Live CD86+ cells
MFI
Comp-APC-A
FMO
0.47%
Control
4.08%
Vehicle
1.96%
Laser alone
3.26%
PBNP alone
4.38%
PBNP-PTT 0.75W
6.23%
PBNP-PTT 1W
24.1%
PBNP-PTT 1.5W
65.0%
PBNP-PTT 2W
53.3%
SSC-A
CD86 (Comp-APC-A)
I
Live HLA-A,B,C+ cells
MFI
Comp-AF 700-A
FMO
0.21%
Control
6.17%
Vehicle
2.83%
Laser alone
4.44%
PBNP alone
5.61%
PBNP-PTT 0.75W
19.8%
PBNP-PTT 1W
68.2%
PBNP-PTT 1.5W
84.0%
PBNP-PTT 2W
65.4%
SSC-A
HLA-A,B,C (Comp-AF 700-A)

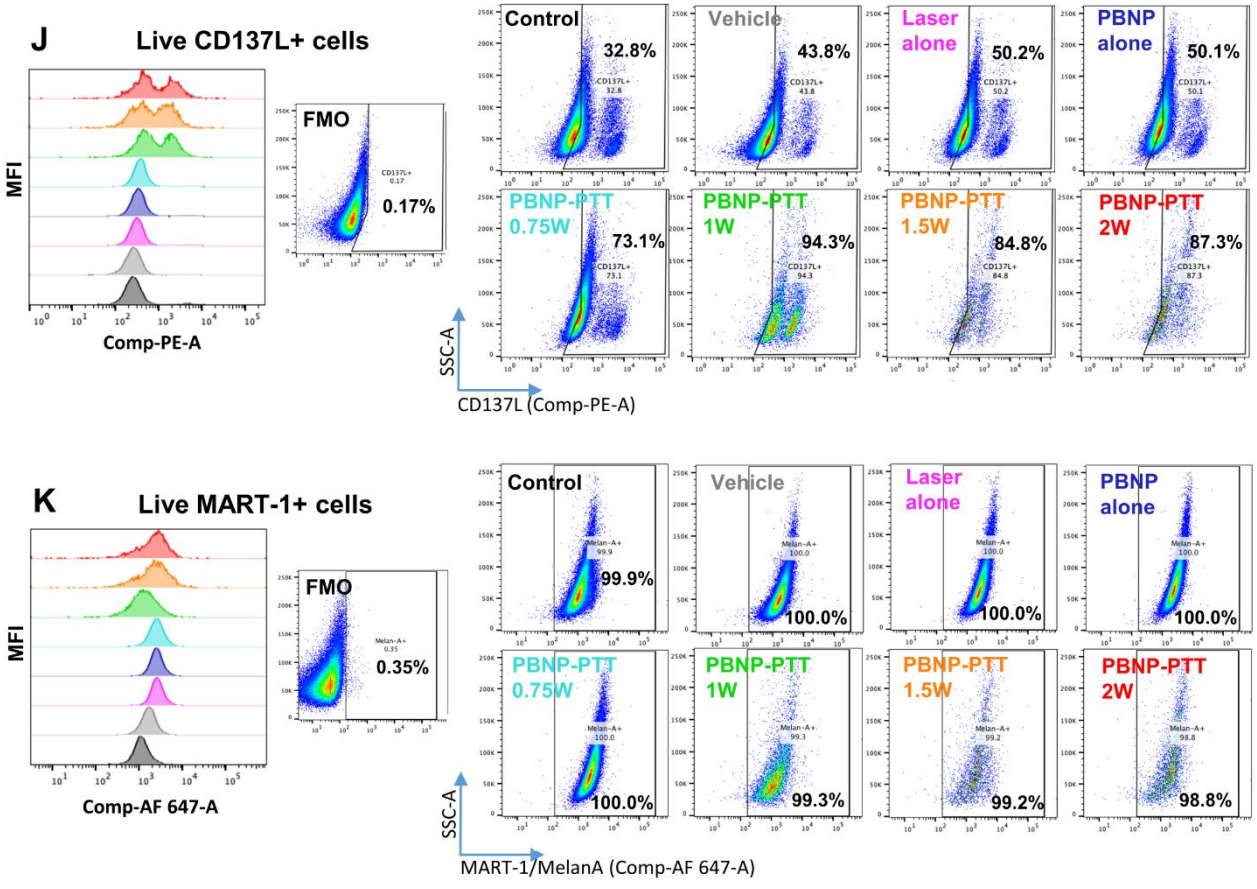

Figure S6 Analysis of WM793 human melanoma cells for expression of ICD and immunostimulatory molecules after PBNP-PTT. A) Temperature curve showing consistent increase in temperature in a laser-power dependent manner with highest temperature of 83.2 °C reached with 2 W PBNP-PTT. B) CEM43 graph indicating increase in thermal dose in a laser-power dependent manner. C) Viability assay by flow cytometry shows WM793 cell death in a thermal-dose dependent manner. D-F) Analysis of molecules associated with ICD (ATP, calreticulin, and HMGB1) showed (D) increased ATP release (indicated by lower intracellular ATP), (E) increased surface calreticulin and (F) decreased intracellular HMGB1 in a thermal dose-dependent manner. G-K) Flow cytometry analysis showing an increase in molecules associated with T cell stimulation, (G) CD80, (H) CD86, (I) HLA-class I (HLA-A,B,C), (J) CD137L, and (K) MART-1 expressed on surface of surviving WM793 human melanoma cells treated with PBNP-PTT at varying laser powers, suggesting increased immunogenicity with increased laser power and thermal dose, consistent with the SM1 murine melanoma model.

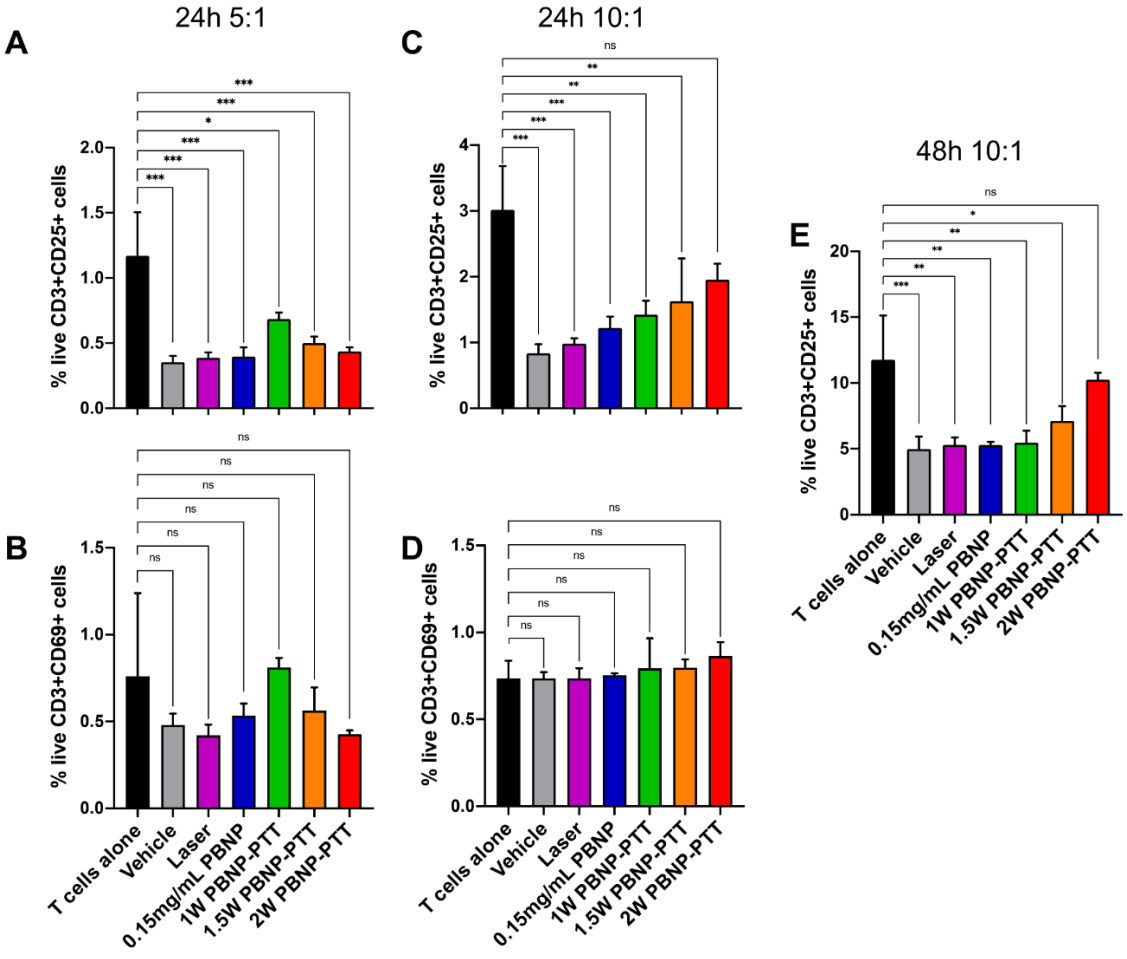

Figure S7 ***Ex vivo*** **T cell activation by PBNP-PTT-treated SM1 cells.** A-E) At an E:T ratio of 5:1, T cells co-cultured for 24 h with SM1 melanoma cells pre-treated with PBNP-PTT showed (A) small but statistically significant changes in CD25 expression at several laser powers studied (0.75 W-2 W), and (B) no changes in CD69 expression. At an E:T ratio of 10:1, T cells co-cultured for 24 h with SM1 melanoma cells pre-treated with PBNP-PTT showed (C) small but statistically significant changes in CD25 at some conditions studied, and (D) no changes in CD69 expression. (E) At an E:T ratio of 10:1, T cells co-cultured for 48 h with SM1 melanoma cells pre-treated with PBNP-PTT showed small but statistically significant changes in CD25 at many conditions studied. Statistical analysis: One-way ANOVA using Tukey's multiple comparison test. ns: not significant, *p< 0.05, **p<0.01, ***p<0.001, ****p<0.0001.

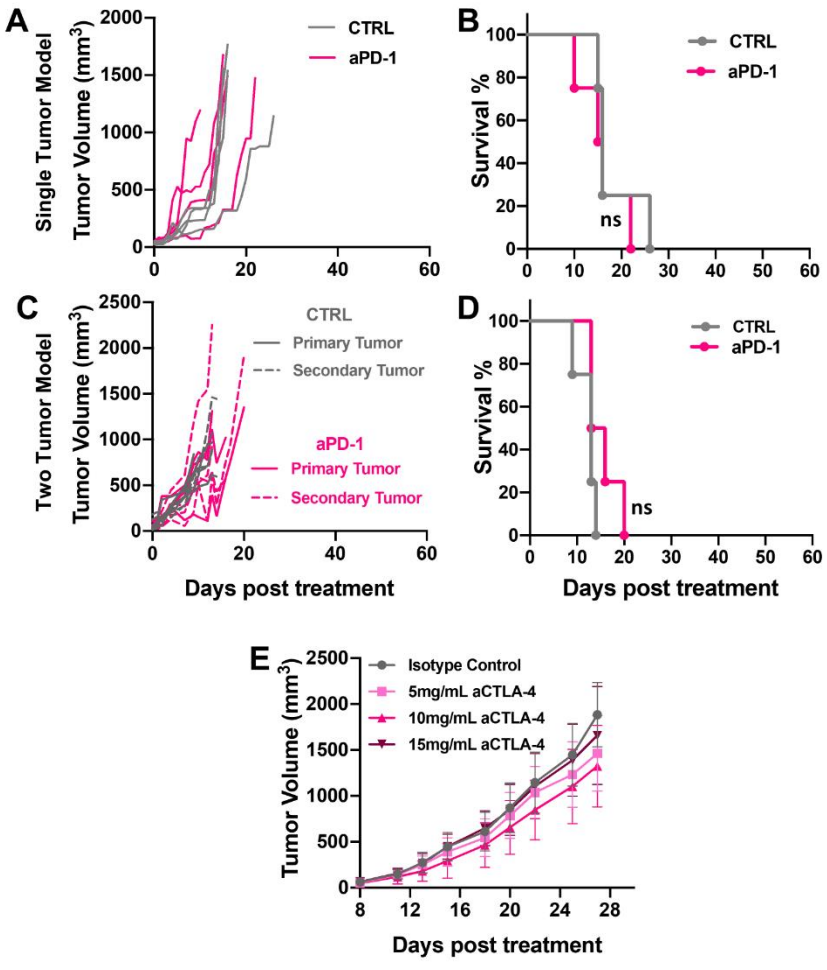

Figure S8 ICI immunotherapy is ineffective to treat SM1 melanoma *in vivo*. A-B) Single SM1 tumor-bearing mice were left untreated (CTRL) or treated with i.p. aPD-1. There was no difference in (A) tumor growth or (B) survival between the groups. C-D) Two synchronous SM1 tumor-bearing mice were left untreated or treated with i.p. aPD-1. There was no difference in (C) tumor growth or (D) survival between the groups. E) Single SM1 tumor-bearing mice were treated with an isotype control and different concentrations (5, 10 and 15 mg mL^{-1}) of aCTLA-4. There were no changes in average tumor growth across the groups. Statistical analysis on survival graph: Log-rank (Mantel-cox) test. ns: not significant; n=4/group.

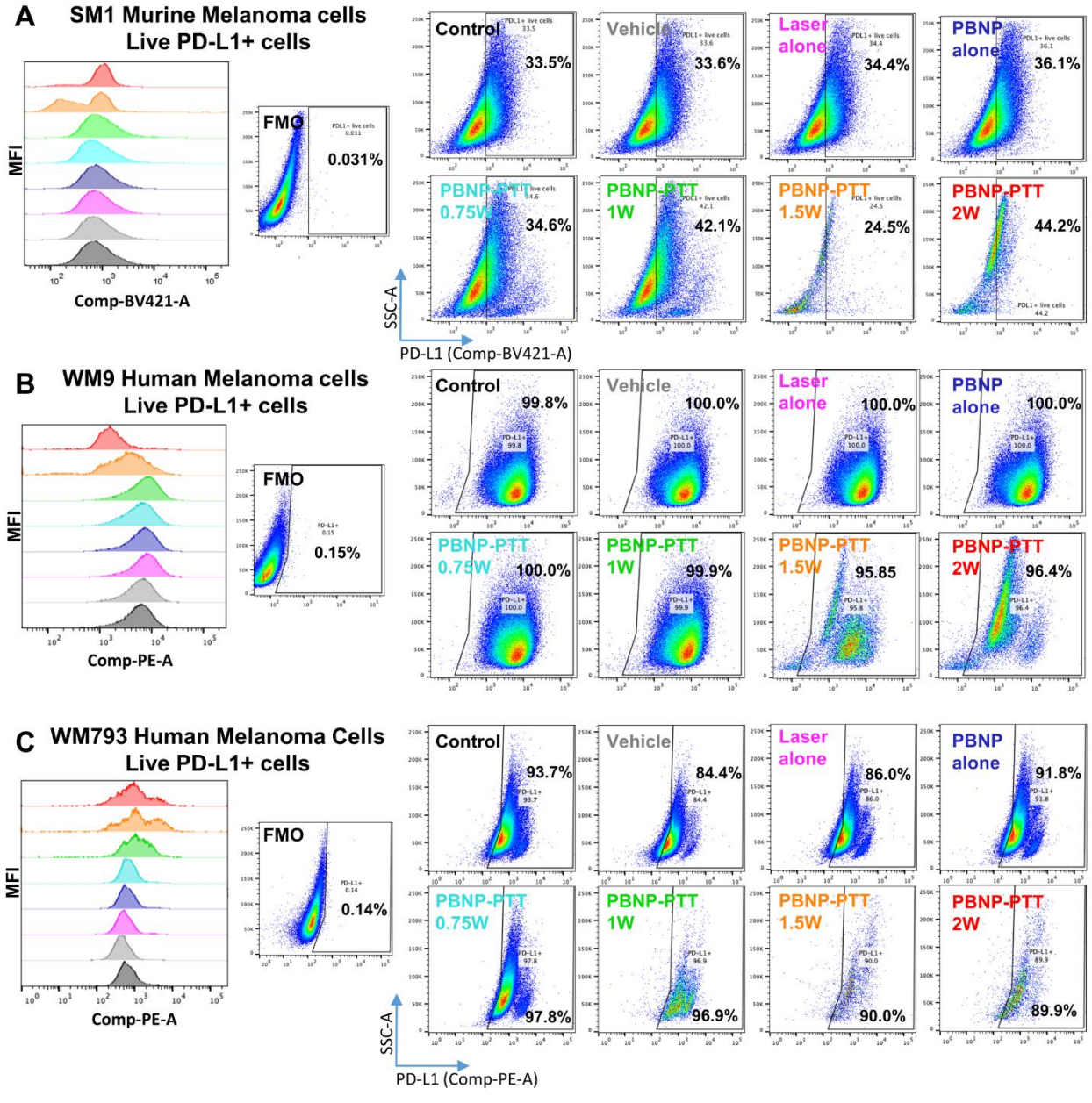

Figure S9 Flow cytometry analysis of melanoma cells for expression of PD-L1 after PBNP-PTT. A) PD-L1 levels were found to be unchanged or decreased from basal expression at all PBNP-PTT conditions in both the mouse SM1 melanoma cells and human melanoma cell lines, (B) WM9 and (C) WM793. These results suggest that aPD-1 therapy may not improve the efficacy of PBNP-PTT.

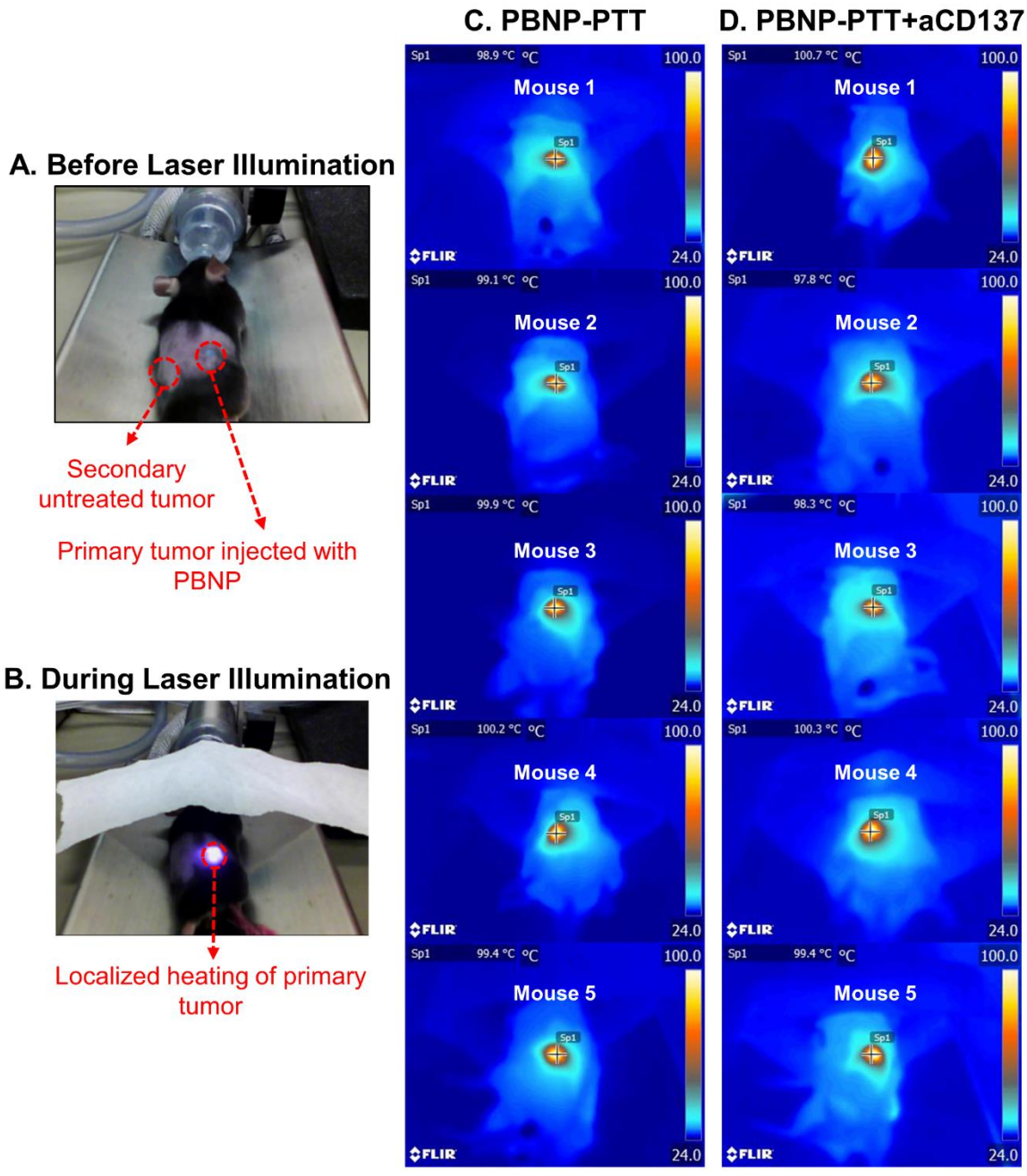

Figure S10 ***In vivo*** **PBNP-PTT setup.** A-B) Digital photographs showing the preparation of C57BL/6 mice carrying two tumors, where (A) one tumor (primary) was injected intratumorally with 50 µL of 1 mg mL^{-1} PBNP and the second tumor (secondary) was left untreated, followed by (B) laser illumination of the PBNP-injected primary tumor with an 808 NIR laser for 10 min. The entire procedure was carried out under general gas anesthesia and the eyes of the animals were covered to protect from damage. C-D) IR images showing the thermal distribution of the tumor (marked by + symbol), indicating the maximum temperature reached during PBNP-PTT. All animals (10 mice shown here) were treated with PBNP-PTT. Post-treatment, the animals were randomly separated into two groups, (C) PBNP-PTT alone and (D) PBNP-PTT + aCD137. The latter group received six i.p. doses of aCD137 over the course of two weeks following PBNP-PTT treatment.

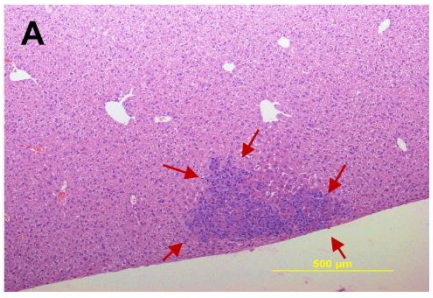

B

Group	# total mice	# mice with liver metastasis	%
CTRL	5	3	60
PBNP-PTT	5	1	20
aCD137	5	3	60
PBNP-PTT + aCD137	5	1	20

Figure S11 Analysis of liver metastasis. A) Representative histology image illustrating SM1 tumor metastasis in the liver (indicated by red arrows). Metastasis was defined as a group of 10 or more tumor cells. B) Table listing the percentage of animals harboring liver metastases in the four treatment groups.

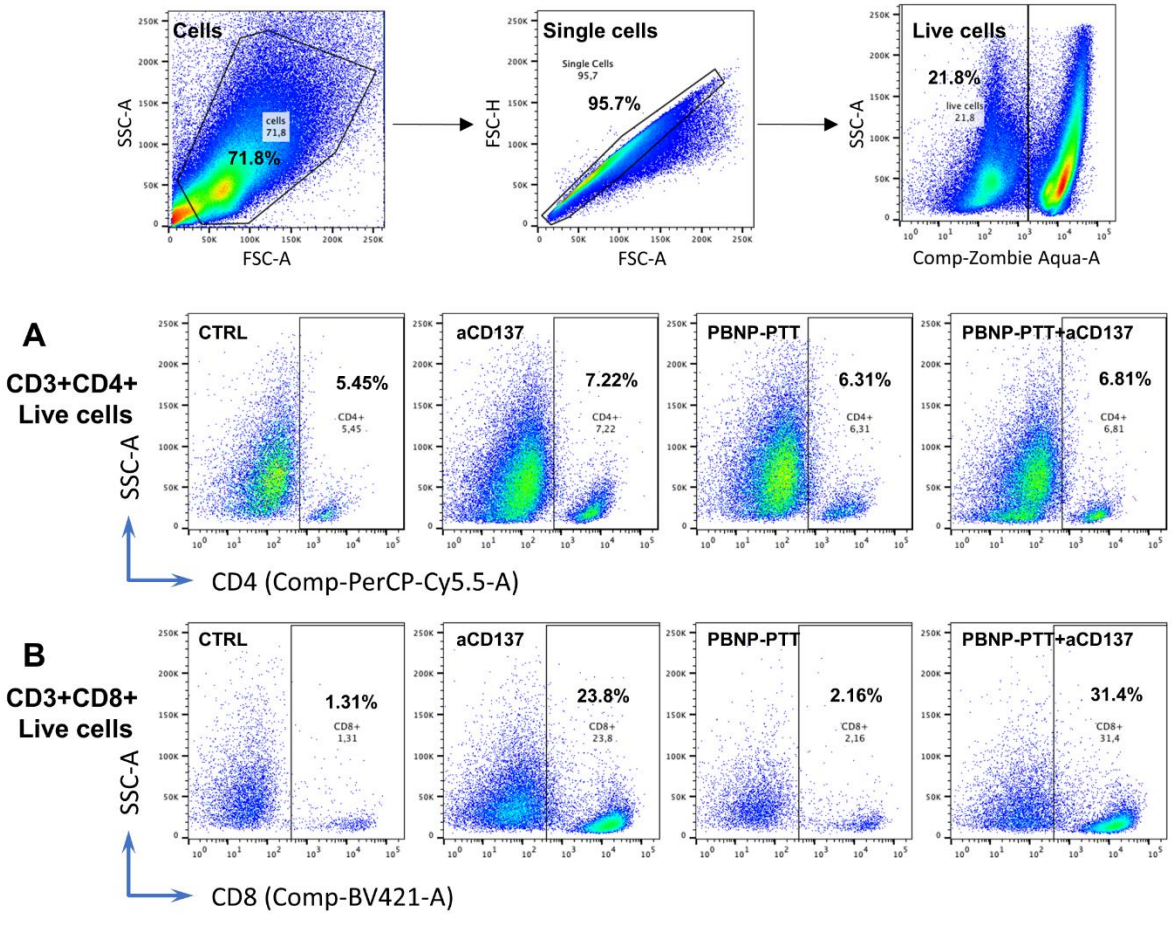

Figure S12 Flow cytometry analysis of secondary untreated tumors for T cells. A) Representative scatter plots showing no change in the levels of CD4+ T cells within secondary untreated tumors of CTRL animals and animals treated with aCD137 alone, PBNP-PTT, or PBNP-PTT + aCD137. B) Representative scatter plots showing a significant increase in CD8+ cytotoxic T cells within secondary tumors in groups treated with aCD137 (aCD137 alone and PBNP-PTT + aCD137) compared to CTRL and PBNP-PTT treatment groups. The average amount of CD8+ T cells was higher in mice treated with PBNP-PTT + aCD137 (i.e. 31.4% depicted here) compared to aCD137 alone (i.e. 23.8% depicted here).

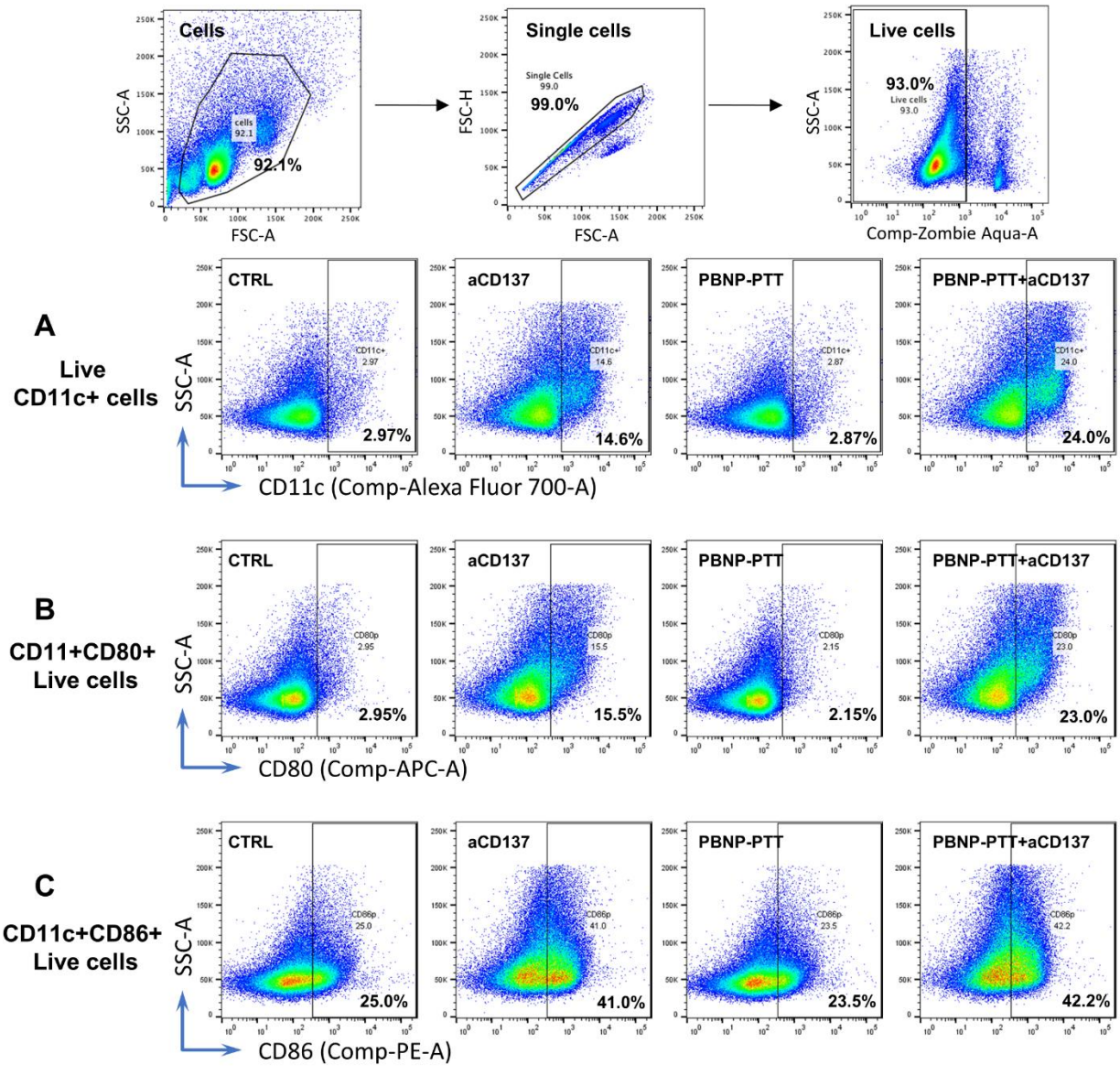

Figure S13 Flow cytometry analysis of lymph nodes for migration and maturation status of dendritic cells (DCs). A) Representative scatter plots showing increased CD11c+ DCs in lymph nodes of animals treated with PBNP-PTT + aCD137 compared to all other treatment groups. B-C) Representative scatter plots analyzing DC maturation markers CD80+ and CD86+ expressed on CD11c+ DCs. There was (B) a significant increase in CD11c+/CD80+ DCs in mice treated with PBNP-PTT + aCD137 compared to all other groups, but (C) no change in CD11c+/CD86+ DCs in lymph nodes of animals treated with PBNP-PTT + aCD137 compared to CTRL.

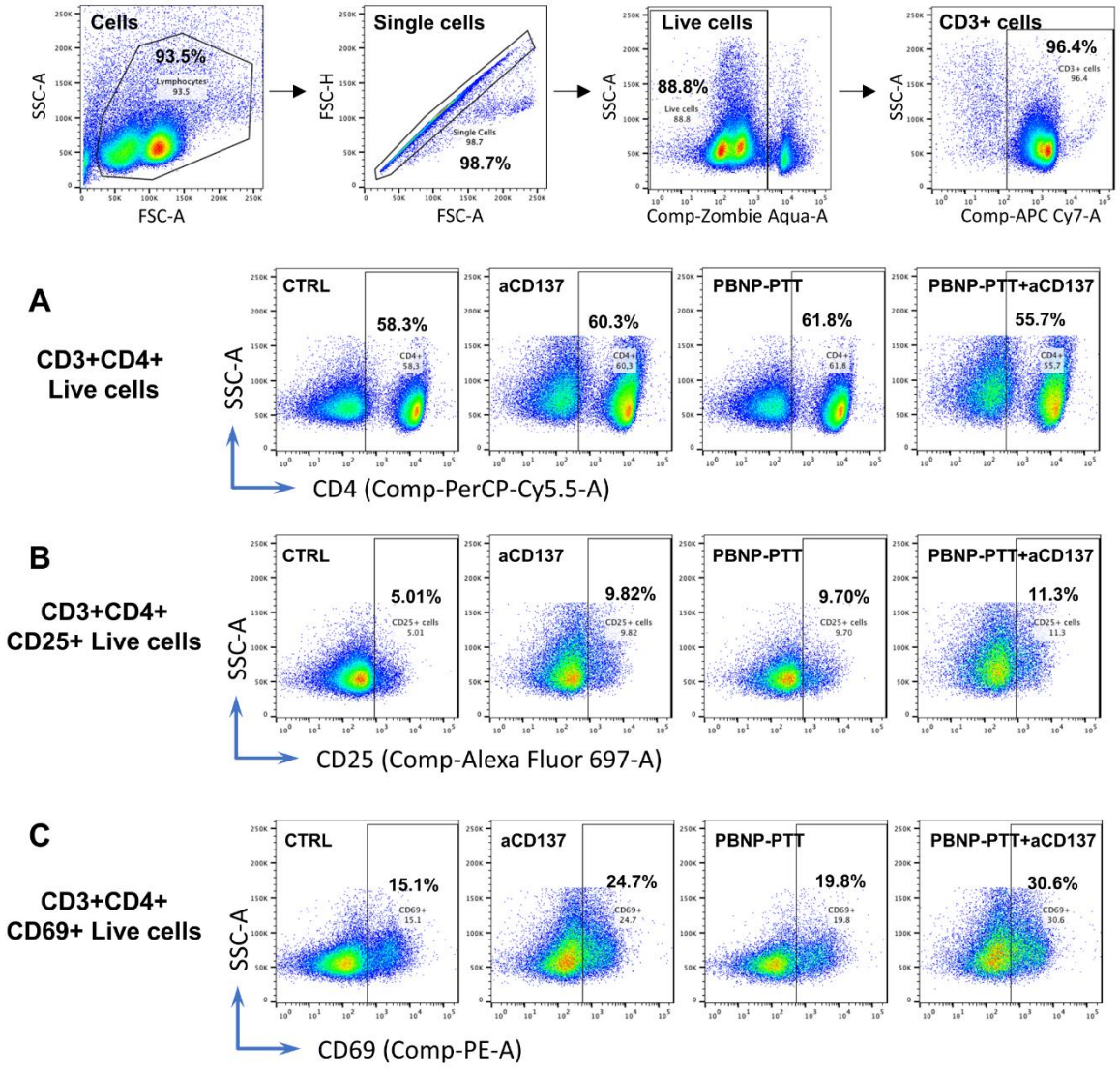

Figure S14 Flow cytometry analysis of CD4+ T cell activation status in the spleen. A) Representative scatter plots showing a mild decrease in CD4+ T cells in the spleens of mice treated with PBNP-PTT + aCD137 compared to CTRL and PBNP-PTT-treated mice. B) Representative scatter plots showing a significant increase in the T cell activation marker CD25 on CD4+ T cells in mice treated with PBNP-PTT + aCD137 compared to CTRL. C) Representative scatter plots showing a significant increase in the T cell activation marker CD69 on CD4+ T cells in mice treated with PBNP-PTT + aCD137 compared to all other treatment groups. This illustrates that despite the decrease in the CD4+ T cell population in mice treated with the combination therapy, the splenic CD4+ T cells were more activated compared to CTRL and monotherapies.

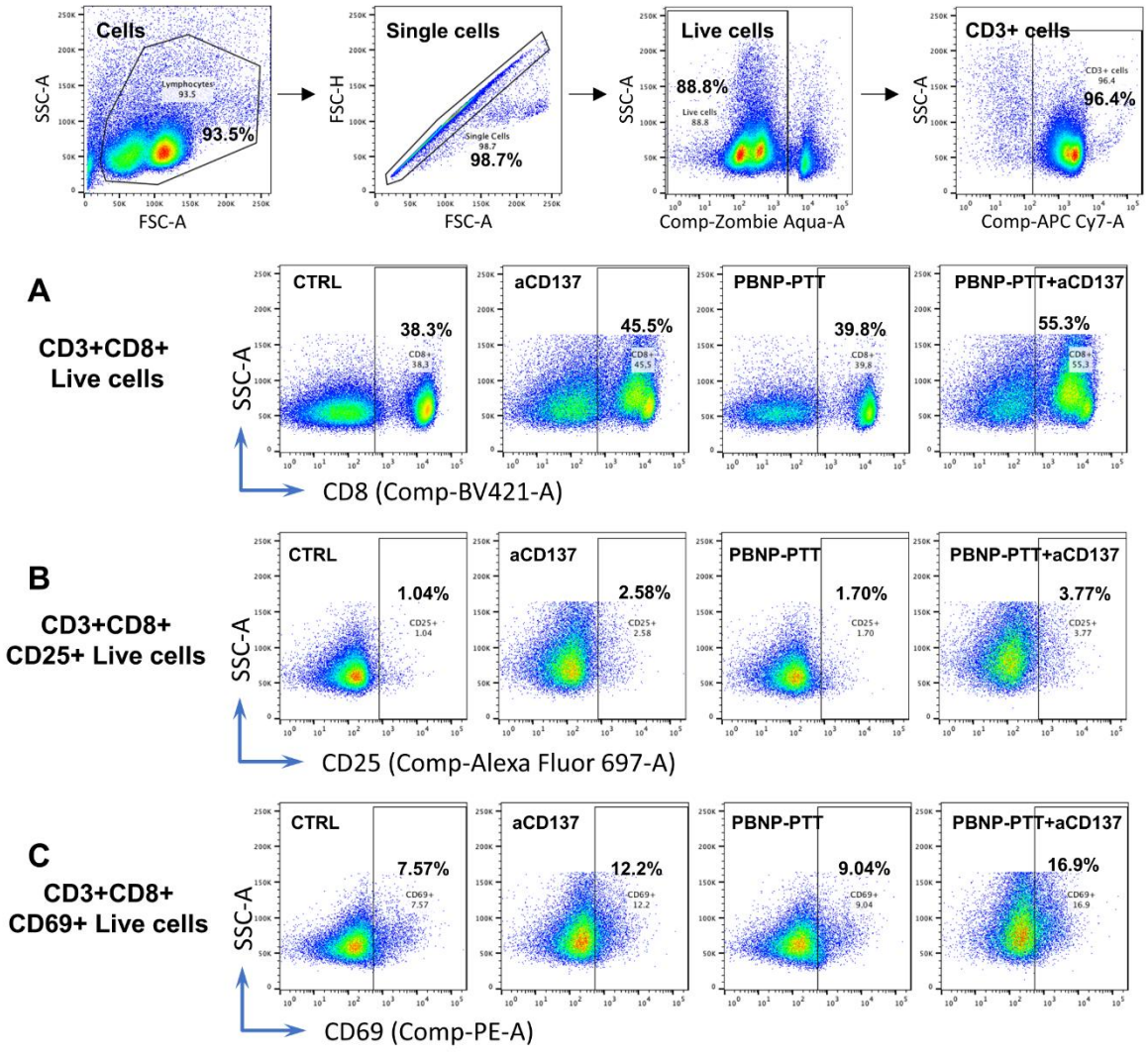

Figure S15 Flow cytometry analysis of CD8+ T cell activation status in the spleen. A) Representative scatter plots showing a significant increase in CD8+ T cells in the spleens of mice treated with PBNP-PTT + aCD137 compared to all other treatment groups. B) Representative scatter plots showing a significant increase in the T cell activation marker CD25 on CD8+ T cells in the PBNP-PTT + aCD137 treatment group compared to CTRL and PBNP-PTT alone. C) Representative scatter plots showing a significant increase in activation marker CD69 on CD8+ T cells for groups treated with aCD137 and PBNP-PTT + aCD137 compared to CTRL.

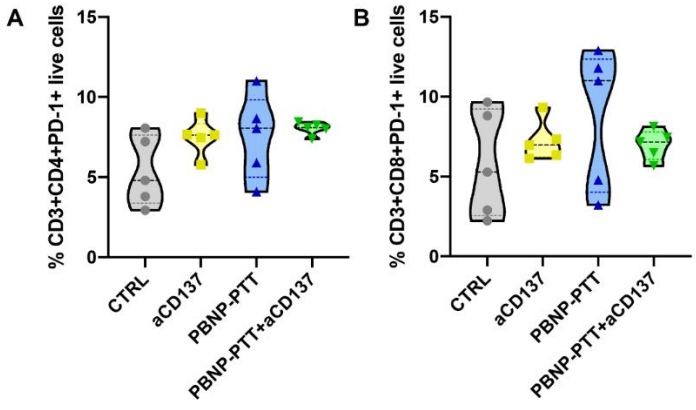

Figure S16 Flow cytometry analysis of exhaustion status of T cells in spleen. A-B) Violin plots illustrating no change in the T cell exhaustion marker, PD-1, on either (A) CD4+ or (B) CD8+ splenic T cells across all treatment groups. Statistical analysis was done using one-way ANOVA, Tukey's multiple comparison test.

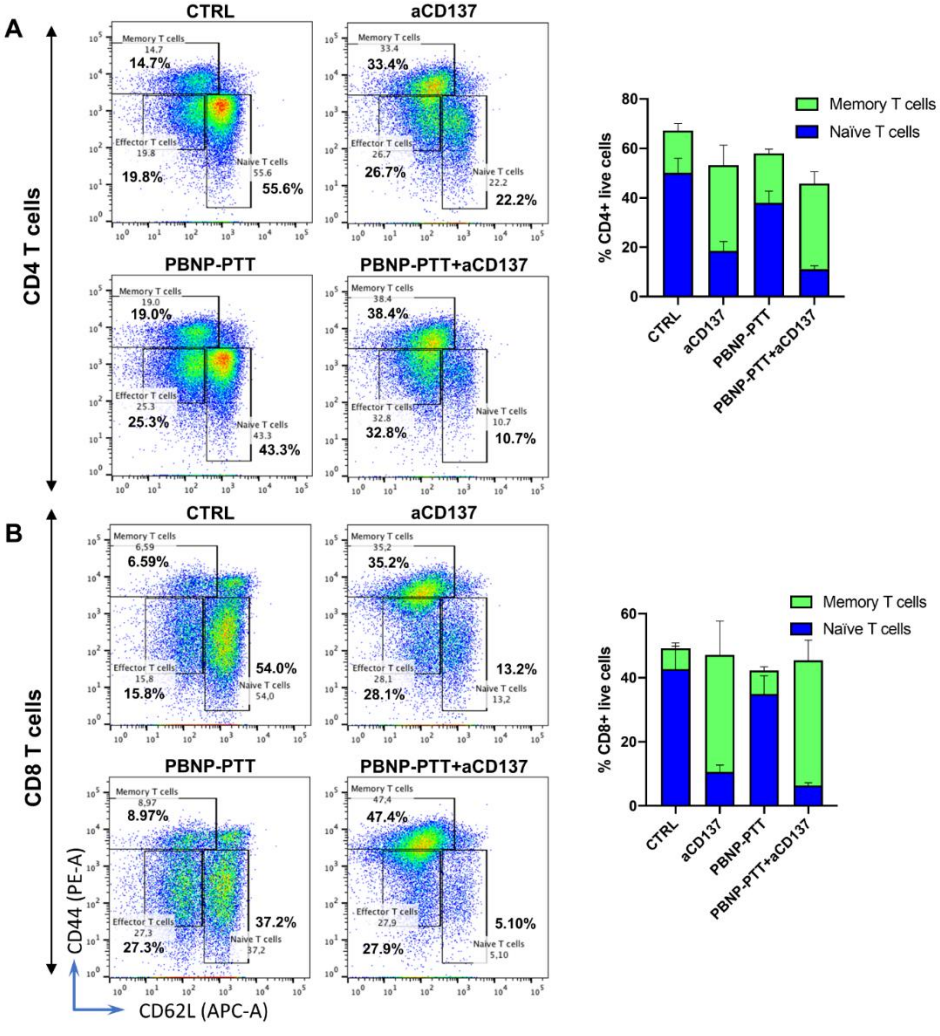

Figure S17 Flow cytometry analysis of naïve vs memory T cells in spleen. A-B) Representative scatter plots showing significant decrease in CD62L+/CD44- naïve (A) CD4+ and (B) CD8+ T cells and significant increase in CD44+/CD62L- memory (A) CD4+ and (B) CD8+ T cells in spleen of animals treated with aCD137 or PBNP-PTT + aCD137 compared to CTRL and PBNP-PTT.

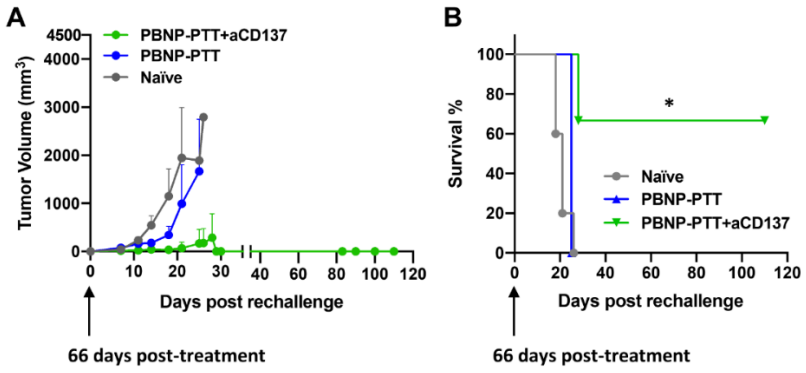

Figure S18 Tumor rechallenge compared to naïve age-matched animals. Long-term surviving animals after single tumor challenge were rechallenged with SM1 tumors on day 66 post-treatment initiation. A) Tumor growth curve shows complete tumor rejection in 2/3 surviving animals previously treated with PBNP-PTT + aCD137, suggesting long-term immunological memory, compared to naïve (0/5 rejection, all challenged animals grew tumors) and PBNP-PTT (0/2 rejection, all rechallenged animals grew tumors). B) Kaplan-Meier plot demonstrating 66% long-term tumor-free survival for PBNP-PTT + aCD137-treated animals up to 110 days post-rechallenge, compared to the naïve and PBNP-PTT group. Statistical analysis was done using Log-rank (Mantel-Cox) test. *p < 0.05.

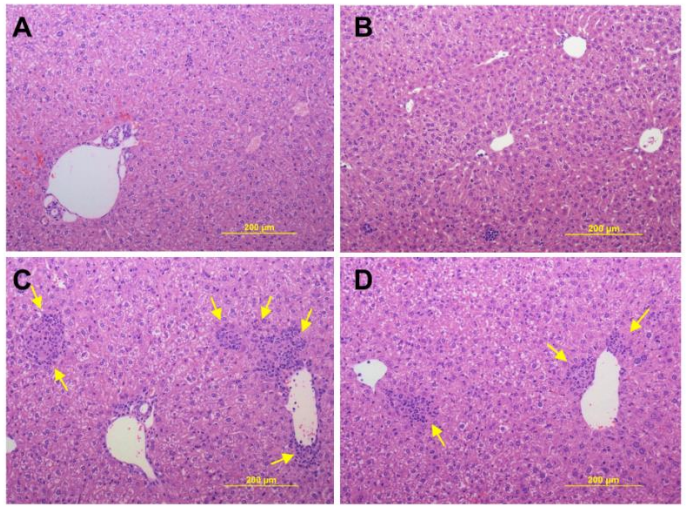

Statistical significance	Lobules	Central vein	Portal tract	Overall
CTRL vs. aCD137	***	***	***	***
CTRL vs. PBNP-PTT	ns	ns	ns	ns
CTRL vs. PBNP-PTT + aCD137	***	***	***	***
aCD137 vs. PBNP-PTT	**	***	***	***
aCD137 vs. PBNP-PTT + aCD137	ns	ns	***	ns
PBNP-PTT vs. PBNP-PTT + aCD137	***	***	***	***

*ns: not significant; ** p < 0.01, *** p < 0.001*

Figure S19 Analysis of acute hepatotoxicity. A-D) Histology sections showing no inflammation in (A) CTRL and (B) PBNP-PTT-treated animals, and clusters of inflammatory cells (indicated by yellow arrows) near hepatic blood vessels in both (C) aCD137 and (D) PBNP-PTT + aCD137-treated animals. E) Livers were scored for inflammation in the lobules, central vein, and portal tracts. Overall inflammation, as quantified across the three examined locations, was also measured, showing increased inflammation in aCD137-containing treatment groups.

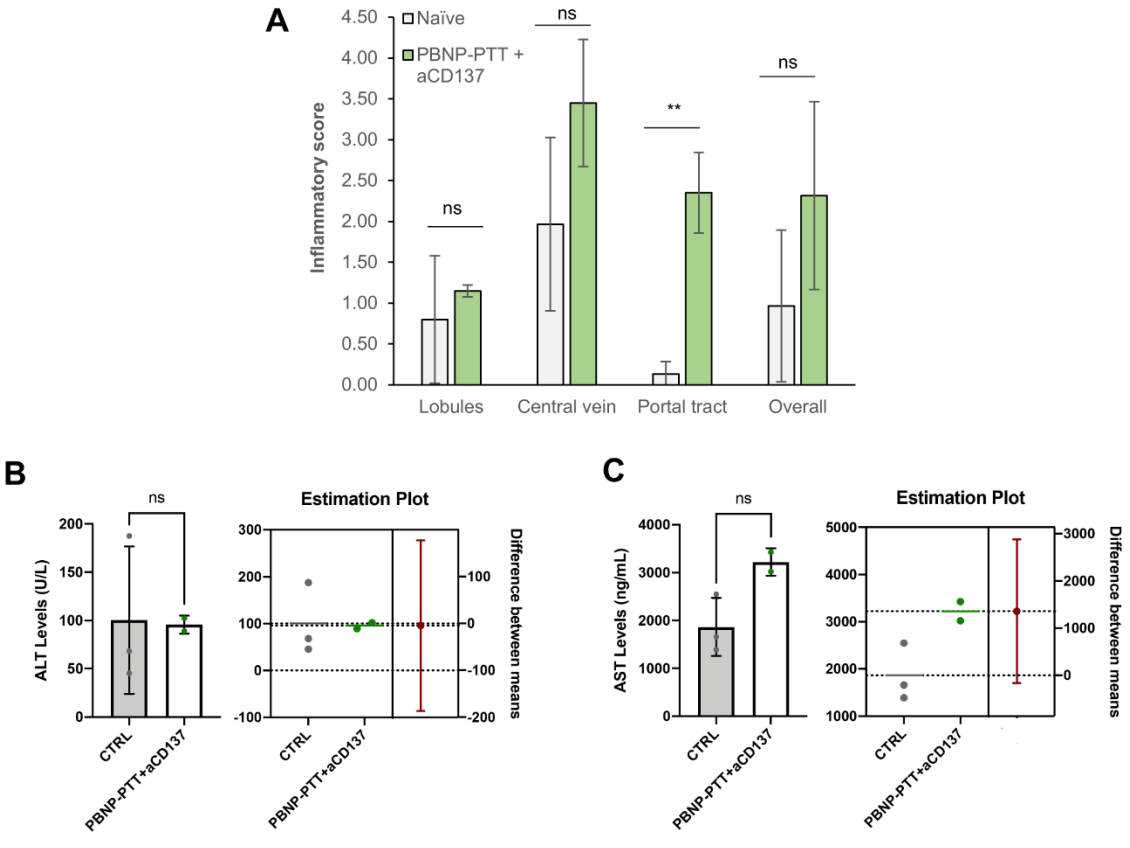

Figure S20 Analysis of chronic hepatotoxicity on long-term surviving PBNP-PTT + aCD137-treated mice. A) Livers from long-term surviving PBNP-PTT + aCD137-treated mice (n=2; green) and age-matched naïve mice (n=3; gray) were scored for inflammation in the lobules, central vein, and portal tracts. Overall inflammation, as quantified across the three examined locations, was also measured. Treated mice showed significantly higher portal tract inflammation (scored as mild inflammation) than controls, but no significant difference in overall liver hepatic inflammation. B-C) Sera analysis of (B) alanine aminotransferase (ALT) and (C) aspartate aminotransferase (AST), showing no significant difference between long-term surviving PBNP-PTT + aCD137-treated animals (226 days post-treatment) (n=2) compared to age-matched naïve animals (CTRL, n=3). Significance was calculated using an unpaired t-test and the respective estimation plots are provided alongside the average ALT/AST levels. Each analysis had 3 technical replicates per animal studied.